Associations Between Blood Markers of the GSH Redox cycle and Brain White Matter Microstructure in Psychosis

Tommaso Pavan[1], Pascal Steullet[2], Yasser Alemán-Gómez[1], Raoul Jenni[2], Zoé Schilliger[2,6], Martine Cleusix[2], Luis Alameda[3,4,5], Kim Q. Do[2], Philippe Conus[3], Patric Hagmann[1], Daniella Dwir[2], Paul Klauser[2,6], and Ileana Jelescu[1]

1. Department of Radiology, Lausanne University Hospital (CHUV) and University of Lausanne (UNIL), Lausanne, Switzerland
2. Center for Psychiatric Neuroscience, Department of Psychiatry, Lausanne University Hospital and the University of Lausanne, Lausanne, Switzerland
3. Service of General Psychiatry, Treatment and Early Intervention in Psychosis Program. Lausanne University Hospital (CHUV), Lausanne, Switzerland
4. Department of Psychosis Studies, Institute of Psychiatry, Psychology and Neuroscience. King's College of London, London, UK.
5. Centro Investigacion Biomedica en Red de Salud Mental (CIBERSAM); Instituto de Biomedicina de Sevilla (IBIS), Hospital Universitario Virgen del Rocio, Departamento de Psiquiatria, Universidad de Sevilla, Sevilla, Spain.
6. Service of Child and Adolescent Psychiatry, Department of Psychiatry, Lausanne University Hospital and the University of Lausanne, Lausanne, Switzerland

Corresponding author: Tommaso Pavan; address: *Centre de Recherche en Radiologie*, PET3, CHUV, Rue du Bugnon 46, 1011, Lausanne, Switzerland ; telephone:+41213146020; fax:+41213146020; email: tommaso.pavan@chuv.ch

Abstract

In groups of patients suffering from psychosis, redox dysregulation was reported in both peripheral fluids and brain. It has been hypothesized that such dysregulation, including alterations of the glutathione (GSH) cycle could participate in the brain white matter (WM) abnormalities in schizophrenia (SZ) due to the oligodendrocytes' susceptibility to oxidative stress (OxS).

In this study we aim to assess the differences between 99 psychosis patients (PT) and 86 healthy controls (HC) in GSH-redox peripheral blood markers: GSH peroxidase (GPx), reductase (GR) enzymatic activities and their ratio (GPx/GR-ratio), evaluating the hypotheses that alterations in the homeostasis of the systemic GSH cycle may be associated with pathological mechanisms in the brain WM in PT. We also consider the hypothesis that different homeostatic states of the system (oxidative vs reductive) may reflect differently into the WM microstructure. To do so, we employ the advanced diffusion MRI methods: Diffusion Kurtosis Imaging (DKI) and White Matter Tract Integrity-Watson (WMTI-W), which provide excellent sensitivity to demyelination and neuroinflammation.

We show that GPx levels are higher ($p=0.00050$) in female participants and modulate the effect of aging on the WM. We found differences between PT and HC in the association of GR and mean kurtosis (MK, $p=0.028$). Namely, lower MK was associated with higher blood GR activity in HC, but not in PT, suggesting that high GR activity (a hallmark of reductive stress) in HC was linked to changes in myelin integrity. Remarkably, GSH-redox peripheral blood markers did not explain the WM anomalies detected in PT.

Introduction

Psychosis and schizophrenia (SZ) present significant challenges for patients, their families, and society[1]. Only partially understood, its etiology is attributed to a multifaceted interplay of genetic, environmental and developmental factors that affect a variety of biological processes[2–7] among which the redox balance[8]. In patients suffering from psychosis, a redox dysregulation is reported in peripheral fluids (i.e., diminished antioxidant capacity, oxidative damage of lipids, DNA and RNA[9–11]) and brain (i.e., lower glutathione (GSH), lower NAD+/NADH ratio[12,13]). The causes of such redox dysregulation and the resulting oxidative stress (OxS) are multifactorial, including compromised energy metabolism, endocrine dysregulation, chronic subclinical inflammation and weakened antioxidant capacities. Anomalies in the GSH redox system, a key antioxidant system for cell protection and detoxification, have been widely observed in SZ[9]. While polymorphisms in genes of the GSH system have been associated with SZ[14–19], meta-analyses also show lower mean levels of GSH in blood[9], and brain[13,20–22] in patients vs. controls. The redox regulation and antioxidant function of GSH acts largely via the GSH redox cycle that involves the GSH peroxidase (GPx) and GSH reductase (GR). GPx neutralizes peroxides by oxidizing GSH into GSH-disulfide (GSSG). In turn, GR reduces GSSG back to GSH. Thus, GPx and GR activities and the GPx/GR ratio inform about the homeostasis of this system. Two out of three postmortem studies have found lower brain GPx in patients vs. controls[20–22]. Meta-analyses suggest that SZ patients tend to display also lower blood GPx than controls[9]. The decrease in peripheral GPx activity seems, however, mostly found in chronic patients[23], with variable levels among early psychosis (EP) patients. Thus, EP patients with worse psychosocial outcomes after a 3-year clinical follow-up displayed significantly higher GPx activity at baseline than those with better outcome[24]. By contrast, there is no evidence of consistent alterations of GR in brain[20] and blood[9].

It has been hypothesized that a GSH deficit could participate to the brain white matter (WM) abnormalities in SZ[25,26], consequential to the oligodendrocytes susceptibility to OxS[27], due to their elevated metabolic activity and high iron content for the production and maintenance of the myelin sheaths[28,29]. The GSH redox cycle is involved in the integrity of WM, from the survival, proliferation and differentiation of the oligodendrocyte precursor cells[26,30] (OPC), to the protection of oligodendrocytes against OxS thanks to high GPx expression[31,32]. A dysregulation of the GSH system will also alter axons' energy metabolism[33] and mitochondrial activity[34]. Furthermore, this dysregulation can lead to subclinical activation of microglia[35], which may in turn affect WM, due to its role in the WM myelin remodeling via OPC recruitment and phagocytosis of myelin debris, de-myelination and remyelination[36]. *Post-mortem* studies on SZ patients have described diminished oligodendrocyte densities in cortical layer III and subcortical areas, presence of swollen or dystrophic oligodendroglia[37–39], adjacent microglia[40], decompacting and splitting of the myelin sheath with inclusions of vacuoles between myelin layers[37–39].

Abnormal WM integrity in EP is also widely reported using *in-vivo* diffusion magnetic resonance imaging (dMRI). DMRI leverages the random motion of water molecules to infer the microstructural properties of the underlying biological tissue[41]. Most studies investigating the psychosis spectrum show widespread increased mean diffusivity (MD) and/or reduced fractional anisotropy (FA)[42–47] with medium effect sizes[46] (*Cohen's d*=0.42), consistent with anomalies described in the *post-mortem* studies. However, the evidence of a link between WM anomalies and the

GSH system in subjects with psychosis remains sparse. GSH levels in frontal brain regions have been found to correlate positively with generalized FA (gFA) in the cingulum of both EP patients and controls[26], while it was shown in earlier work that the precursor of GSH and antioxidant, N-acetylcysteine (NAC), improves the integrity of the fornix (i.e., increases gFA) in EP patients[48] and increases brain GSH[49].

Here, we aim to assess in patients with psychosis whether the activity of GPx, GR, and the GPx/GR ratio measured in blood cells (which inform about the systemic homeostasis of the GSH redox cycle) are associated with the WM microstructure estimated using dMRI. For this purpose, we utilized advanced dMRI methods: Diffusion Kurtosis Imaging[50,51] (DKI), an extension of the diffusion tensor imaging (DTI), and the biophysical model White Matter Tract Integrity-Watson[52,53] (WMTI-W). In addition to classical DTI measures such as MD and FA, DKI enables the estimation of the mean kurtosis (MK), a measure of diffusion variance within each voxel arising from heterogeneous sub-domains, such as cellular compartments, which provides complementary information about tissue heterogeneity. The WMTI-W model allows the estimation of specific microstructural cellular features such as the axonal density (f) in each voxel, with less *ad hoc* simplifying assumptions, less fit constraints[54,55] and increased validity[55] as compared to other biophysical methods such as free-water imaging[56] (FWI) and Neurite Orientation Dispersion and Density Imaging[54] (NODDI). We focused our analysis on these four metrics (MD, FA, MK, f) because of their ability at detecting abnormal myelination or demyelination[57–60] (↑MD, ↓FA, ↓MK, ↓f), but also neuroinflammation which has the effect of reducing diffusivities (↓MD, ↓FA) and increasing kurtosis and apparent axonal water fraction (↑MK, ↑f) due to higher cellular crowding associated with microgliosis and astrocytosis[57,58,61,62]. In a recent study, we have shown an increase in MD and a decrease in FA, MK and f in the WM of patients with psychosis when compared to age range-matched controls, with these alterations being surprisingly more pronounced during the first years of psychosis[63].

Here we hypothesize that alterations in the homeostasis of the systemic GSH redox cycle may be associated with pathological mechanisms in the brain (i.e., redox dysregulation and microglia dysfunction) that affect WM. Therefore, we expected that peripheral markers related to the GSH redox cycle may correlate with some of the WM microstructure metrics, sensitive to neuroinflammation and myelination, as previous treatment studies targeting the GSH redox system via NAC have shown an increase in brain GSH[49] and improvement of gFA in the fornix[48]. We also anticipate that relationships between the GSH redox cycle and WM differ in healthy controls (HC) and patients, but also between subgroups of participants classified as having low GPx/GR-ratio versus high GPx/GR-ratio.

Methods

Participants

Data were collected from 185 individuals (**Table 1**) divided into two groups: 86 healthy controls (HC), 99 patients (PT) with a diagnosis from the psychosis spectrum (**Supplementary Table S1**). Patients that suffered at least one psychotic episode (as defined by Comprehensive Assessment of At-Risk Mental States scale[64], CAARMS) or had DSM-IV diagnosis of SZ and schizoaffective disorder were recruited from the Lausanne University Hospital. PT with psychosis related to intoxication or organic brain disease, IQ<70, reporting alcoholism, drug abuse, major somatic disease, documented anamnestic or current organic brain damage were excluded. HC were recruited from the same sociodemographic area as the patients. HC were excluded if they had a first-degree family member who suffered from psychosis or prodromal symptoms, or if they reported current or past antipsychotic treatments. Symptoms in PT were assessed via the Positive and Negative Syndrome Scale[65] (PANSS), and global functioning was estimated for the whole sample via the Global Assessment of Function[66] scale (GAF). The study was approved by the local Ethics Committee of the Canton of Vaud (Switzerland) under authorization numbers CER-VD 382/11 and 2018-01731.

MRI acquisition

MRI scanning sessions were performed on two different 3-Tesla systems (Magnetom TrioTim and PRISMA, Siemens Healthineers, Erlangen, Germany), each equipped with a 32-channel head coil. A 1-mm isotropic T1-weighted image was acquired for anatomical reference. Whole-brain diffusion-weighted images (DWI) were acquired using diffusion spectrum imaging (DSI) scheme across 15 b-values, ranging from 0 to 8000 s/mm^2, spatial resolution of 2.2 x 2.2 x 3 mm^3 - See Supplementary Material for further acquisition details.

Image preprocessing

The MPRAGE image was bias field corrected[67] and skull-stripped via nonlinear registration to the MNI-152 template[68] using Advanced Normalization Tools[69] (ANTs). The diffusion preprocessing pipeline included MP-PCA denoising, Gibbs ringing-, EPI-, eddy current and motion corrections, following most recent guidelines[70] - see Supplementary Material for preprocessing details.

Microstructure estimation

For DKI and WMTI-W estimation, the diffusion dataset was truncated[50] at b≤2500 s/mm^2. DKI was fit voxel-wise in the entire brain[71] using a weighted linear-least squares algorithm in Matlab[71], from which seven scalar maps were derived. Four from DTI: RD, MD, AD and FA, and three from DKI: radial, mean, axial kurtosis (RK, MK, AK). However, only three parameter maps were included in the statistical analysis: MD, FA, and MK. WMTI-W parameters were estimated voxel-wise from the seven DKI scalars, using an in-house Python script, yielding five parameter maps: axonal density f, intra-axonal diffusivity D_a, extra-axonal parallel and perpendicular diffusivities $D_{e,//}$, $D_{e,\perp}$ and axon orientation alignment c_2. However, only axonal density f was included in the statistical analyses, to limit the number of comparisons.

Blood analyses

GR and GPx activity were assessed in hemolyzed blood cells incubated in phosphate buffer solution (100mM, pH 7.5) containing EDTA (0.6mM), and non-limiting levels of either oxidized glutathione (GSSG, 2.5mM) and NADPH (0.25mM) (for GR), or GSH (2.5mM), NADPH (0.25mM), GR (0.84U/ml; Fluka) and tert-butyl hydroperoxide (TBHP, 0.8mM, Fluka) (for GPx). We expressed GPx and GR activities in nmoles NADPH used/min/g hemoglobin. These enzymatic activities were measured with two different plate readers. Batch effects between plate readers were corrected via Combat for biological data[72] (see additional details on the blood analyses and harmonization procedure in the supplementary material).

Statistical analysis

Blood markers analysis

Statistical analyses were run in R[73], group comparisons were computed via Welch's t-test and ANOVA. Robust linear regression[74] was used for all the regression and contrasts analyses, always including a correction by (quadratic) age, sex. Post-hoc pairwise contrasts were multiple comparisons corrected via False-Discovery Rate (FDR).

Evidence about the influence of aging on the redox system has been reported in the literature[75,76], suggesting the system is maintained until ~45 years of age[76]. We evaluated this hypothesis first by considering age as a continuous variable and then by comparing subjects under and above 40 years old ($N_{<40y.o.}$=165, $N_{\geq 40y.o.}$=21).

Association between blood markers and WM microstructures

Before any statistical analysis, all the microstructure parameter estimates were harmonized for scanner type via ComBat harmonization[77], which was proven efficient at correcting scanner effects in the same cohort[78]. Furthermore, participants with a delay between MRI scan and blood samples larger than 60 days were excluded whenever an association between blood biomarkers and WM microstructure metrics was tested (84% of the original cohort, N_{HC}=80, N_{PT}=76, $delay_{HC}$=10.0±11.7, $delay_{PT}$=19.0±16.0, p<0.0001). All analyses included a correction for (quadratic) age, sex, and delay. Associations were initially tested at a whole WM level and then at voxel level using FSL's Tract-Based Spatial Statistics[79] (TBSS). First, individual FA maps were used to build a study-specific FA template using ANTs[69] and the estimated warps were used to spatially normalize each individual FA, MD, MK and f map. From the average FA, a WM skeleton was estimated and warped-back to native space where individual FA, MD, MK, and f averages were computed for the whole WM skeleton analysis. While, at voxel level, the skeleton voxels were harmonized in template space with ComBat[77] before permutation testing (FSL randomise[80], 5000 permutations). The resulting statistical maps were FDR and Threshold-Free Cluster Enhancement (TFCE) corrected.

Low and High GPx/GR ratio analysis

To study if there could be differences between participants showing different levels of GPx and GR activity, we repeated the analysis described above after re-classifying the participants into two groups according to their GPx/GR-ratio. Low-ratio and high-ratio were defined as having a GPx/GR-ratio respectively lower and higher than the median GPx/GR ratio of the HC group (**Fig.1A,** $Median_{HC}$=6.64).

Results

Demographics

Summary demographics of the cohort can be found in **Table 1**. PT (29±9 y/o) and HC (28±8 y/o) did not differ in age (p=0.39). Differences were found between PT and HC in functional levels as measured by the GAF scale (p<0.0001)

and in the delay between MRI acquisition and blood collection (p<0.0001), leading to the inclusion of this variable as covariate.

GSH-redox cycle system

Overall, GPx (p=0.60) and GR (p=0.19) activities or the GPx/GR-ratio (p=0.39) did not differ between PT and HC groups. When pooling together HC and PT, female participants showed higher GPx activity than males (p=0.00050). GPx and GR activities correlated significantly for the whole cohort (r=0.38, p<0.0001, **Fig. 1A**), but also for PT (r=0.35, p<0.0001) and HC (r=0.40, p=0.00013) when considered independently. The slope contrast between PT and HC did not show any significant difference (p=0.72, **Fig. 1B**). GPx and GR activities correlated also in both males and females (respectively, r=0.47, p=0.00024 and r=0.37, p=0.00037) with no significant sex difference for the slopes either (p=0.15, **Fig. 1C**). Age was only found significantly associated with a decrease in GPx activity (p=0.026). This decrease was particularly significant in participants over 40 years old. This group displayed lower GPx levels (p=0.00083) and ratio (p<0.0001, but not GR, p=0.89) when compared to under 40 years old. Finally, GPx activity and GPx/GR-ratio were found negatively associated with the duration of illness in PT (p<0.0001) but not with age at psychosis onset or medication.

Associations between GSH-redox cycle and WM microstructure

Within the whole cohort, irrespective of the clinical status or sex, neither GPx, GR, or their ratio correlated with average WM skeleton values of MD, FA, MK, or *f*. When considering the clinical status, GR regression models with MK (p=0.028, **Fig. 2A**) and *f* (p=0.043, **Fig. 2B**) showed significant differences between HC and PT slopes. The GPx/GR-ratio association with *f* also showed a difference between HC and PT slopes (p=0.027, **Fig. 2C**), while a trend could be observed for MK (p=0.054). No significant differences between HC and PT were found for GPx association with either MD, FA, MK or *f*.

TBSS analysis of the same regressions further substantiates the relationships of GR with MK but not the associations of *f* with GR or the GPx/GR-ratio. In HC, MK was significantly and negatively associated with GR in multiple WM clusters (**Fig. 2D**). Furthermore, the slope (GR–MK) in HC differed significantly from the one in PT (**Fig. 2E**). The significant contrast was localized bilaterally in the superior corona radiata (CR), genu and body of the corpus callosum (CC).

Associations between GPx, age, sex and WM microstructure

In light of the negative association between GPx levels and age, we also evaluated whether their interaction could be reflected in the WM microstructure. Irrespectively of the clinical status, the interaction model of GPx and quadratic age, corrected for sex and delay, resulted in a significant interaction for MD (p=0.0017, **Fig. 3**). Namely, with aging, MD was overall higher in individuals with low GPx activity than in individuals with elevated GPx activity, irrespective of the clinical status. We also considered the 3-way interaction of GPx, aging, and clinical status on the association with MD, but we did not find any significant interaction (p=0.18). Complementary TBSS analysis did not show any significant cluster for the same regressions.

Low GPx/GR-ratio versus high GPx/GR-ratio

We expected individuals with high GPx/GR-ratio to have a more oxidized redox state of the GSH/GSSG couple than those with a low GPx/GR-ratio. The highest GPx/GR-ratios may indicate systemic OxS, while the lowest GPx/GR-ratios may reflect the presence of reductive stress.

PT were distributed equally between the low-ratio and a high-ratio group (**Table 1**), indicating no overall differences between PT and HC. First, we established that the low- vs high-ratio is driven by both GPx and GR levels. Considering both PT and HC together, participants with low ratio (p<0.0001) had significantly lower GPx (μ_{GPx}=13.09) and higher GR (μ_{GR}=2.61) as compared to subjects with high ratio (μ_{GPx}=19.76, μ_{GR}=2.16). The same pattern was observed within the clinical groups and sex (p<0.0001). GPx and GR significantly correlated within both low- (r=0.65, p<0.0001) and high-ratio (r=0.74, p<0.0001) groups, but their slopes significantly differed (p=0.036) suggesting a tighter coordination of GPx and GR in the high-ratio group. Pairwise contrasts between the slopes of the interaction models of low- and high- ratio with the clinical status (6 tests) did not yield significant results.

Associations between GSH-redox cycle and dMRI WM microstructure in the low and high GPx/GR-ratio groups

We then assessed how low and high GPx/GR-ratio reflected at the WM microstructure level. Overall, the WM metrics did not significantly differ between individuals with low and high ratio after correcting for quadratic age, sex and delay. Two-way interaction models of low- and high- ratio with either sex or clinical status did not yield significant differences. However, the 3-way interaction model of MK (low- and high- ratio, sex and clinical status) showed a significant interaction in GPx ($p=0.012$) and a trend for GR ($p=0.080$). *Post-hoc* comparisons (4 tests: low- vs high-ratio, and PT vs HC) of the two MK models found significant differences in the slopes of GPx ($p_{fdr}=0.038$, **Fig. 4A**) and GR ($p_{fdr}=0.016$, **Fig. 4B**) in low-ratio HC vs low-ratio PT.

TBSS voxel-wise analysis of the same 3-way interaction model showed widespread significant differences in the slopes of MK vs GR between low ratio HC and PT (**Fig. 4C**) but not for any other comparison, indicating the low-ratio group drives the difference between HC and PT. Identified areas for the GR-MK association were the bilateral cerebellar peduncle (CP), internal capsule, the splenium and body of the CC, the whole CR, the right superior longitudinal fasciculum (SLF), right tapetum, genu of the CC, thalamic radiation, fronto-occipital fasciculum (FOF), and the fornix. Notably, many voxels of the peripheral WM were also significant.

Discussion

In this work, we quantified peripheral biomarkers of the GSH redox cycle (GPx, GR activities and their ratio) in patients with psychosis and control subjects, and we explored the relationships of these redox markers with the WM microstructure estimated with advanced dMRI methods. We did not find significant differences in GPx, GR or GPx/GR-ratio between groups. However, female participants showed higher GPx activity than males, independently of their clinical status. GPx was also the only biomarker whose activity decreased with age. Regarding the WM metrics (MD, FA, MK, *f*), only MD changed significantly with aging, with the older subjects displaying in higher MD at lower GPx. Finally, GR activity was negatively associated with MK in HC, but not in PT, mostly driven by the subgroup of individuals with a low GPx/GR-ratio where the differences between HC and PT was considerably enhanced and more widespread across the WM.

Peripheral GSH redox cycle

Many studies have investigated blood GPx and GR activities in cohorts of psychotic patients[9,22,23,81], sometimes with mixed results. However, meta-analyses[9,23] show overall significantly lower GPx, but not GR, in PT as compared to HC. To our knowledge, the GPx/GR-ratio has not yet been examined. The analysis of Flatow et al.[23] indicates that a decrease in GPx activity was prevalent in patients with chronic SZ or in PT with acute relapse but not with first psychosis episode. In our cohort, which includes PT with early psychosis or chronic SZ, we did not find any difference between PT and HC regarding GPx, GR and their ratio, even after correction for age and sex. However, we observed higher GPx activity in females than males and decreased GPx activity with aging (particularly above 40 years old), independently of the clinical status. Thus, some of the discrepancies among studies on PT with psychosis could be explained, not only by the stage of the disease, but also by overlooked effects on the peripheral markers of aging[76,82,83], sex[84], medication[85] and circadian rhythm (see [8] supplementary), methodological differences in sample collection, processing, storage, and quantification. However, our findings of sex and age effects on blood GPx activity, regardless of the clinical status, corroborate results from numerous studies[76,82–84,86]. Higher levels of GPx, but not GR, have been also widely reported in the brain of females as compared to males in both animals and humans[87–89]. A higher GPx activity in females is consistent with more efficient antioxidant systems and less basal inflammation in females than in males[87]. Our observation of a diminished GPx activity with age is also in line with the literature[75] and with the notion that the antioxidant defenses weaken over the years, contributing to the accumulation of OxS and its harmful effects[83]. In our work, we found that GPx and GR activities correlated positively within both PT and HC and within both males and females, suggesting a generally quite well-coordinated GSH redox cycle. Of note, the activity of both enzymes correlated in female, adolescents only from the general population[84], but not in EP patients who had been exposed to childhood trauma[90]. This suggests that the relationship between GPx and GR activities may differ in a sex-dependent manner during adolescence but also among subgroups of individuals according to environmental and other yet unidentified factors. Elevated GPx/GR-ratio and/or GPx activity in blood cells may reflect a condition of systemic OxS, while low GPx/GR-ratio and/or high GR activity may indicate systemic reductive stress. Of note, PT who benefited from a NAC treatment were mostly those with high blood GPx activity[48]. On the other hand, reductive stress is the result of a shift of the redox balance in biological redox couples (i.e., GSSG/GSH, or NAD+/NADPH) to a more reducing state. This reductive stress can disturb redox-sensitive biological processes, but also lead

paradoxically to increase mitochondrial reactive oxygen species (ROS) production, thus overwhelming the ROS neutralization capacity and causing mitochondrial dysfunction and oxidative damage[91]. Of note, PT with SZ younger than 40 years-old were reported to display signatures of reductive stress as compared to age-matched HC[12].

Associations between peripheral GSH redox cycle and WM microstructure

Due to the diversity in the GSH redox cycle status across individuals and the complex effects of sex and age, it was therefore essential to tackle the relationships between the peripheral redox markers and WM microstructure by carefully considering age, sex and their interactions, and by investigating the links between the GSH redox cycle and WM separately in subgroups of individuals characterized by different peripheral redox profiles.

Thus, we first found that MD (the average diffusion coefficient in the tissue) was predicted by the interaction between GPx and aging. MD has been shown to increase in WM with normal aging[92], due to the reduced numbers of myelinated axons, inefficient remyelination processes, increased number oligodendrocytes and excessive myelination around some axons[93].

Our results suggest that GPx may modulate the effect of aging on the WM microstructure as reflected by MD. We found that individuals with low GPx activity tended to display higher MD than subjects with high GPx activity with aging, independently from the clinical status (**Fig. 3**). This is consistent with the antioxidant effect of GPx and with the idea that OxS may contribute to accelerated aging in SZ[94]. We believe the reason for the lack of differences between PT and HC in this association is the sparsity of subjects above 40 years old ($N_{>40y.o.}$=21) which makes the modelling at older ages challenging.

The strongest differences between PT and HC were found in the association of GR with the WM microstructure (**Fig. 2, 4**), particularly with MK. MK is considered a measure of tissue complexity[50,51], which has demonstrated sensitivity at detecting abnormal myelination[57–60], neurodegeneration and neuroinflammation[61]. Our previous work on the same data focusing on JHU region-of-interest (ROI) analysis demonstrated that MK was significantly lower in EP and chronic SZ as compared to age-range matched controls[63]. Our current analyses on the average WM skeleton and voxel-wise on the skeleton revealed that lower MK was associated with higher blood GR activity in HC, but not in PT. This suggests that high GR activity was linked with changes in myelin and tissue heterogeneity in HC. As high GR activity may be sign of reductive stress, we looked at the relationship between GR and MK in individuals with low GPx/GR-ratio. This revealed that the difference in the GR-MK association between PT and HC were indeed mostly driven by individuals displaying a low GPx/GR-ratio. This suggests that reductive stress in blood is linked to a low MK in WM of HC, while this does not appear to be the sole modulator of MK in PT. Here, the lack of a direct association between MK and GR in PT could suggest there are multiple mechanisms affecting WM integrity in PT, and thus a less direct relationship than in HC.

Prior research has shown that NAC treatment can improve brain GSH levels after six months[49] and WM integrity as measured by gFA in PT[48]. Notably, improvements in cognitive abilities and in symptoms[49], particularly in individuals with high GPx levels, have also been reported, highlighting the interplay between blood markers, WM integrity and cognitive function. However, we found no associations between GPx or high-ratio GPx with WM microstructure in PT, contrary to our expectation, further substantiating the possibility that multiple mechanisms are influencing the WM integrity in PT.

As a side note, while we found group differences in WM microstructure metrics at the JHU ROI level and their ensemble in our prior research[63], here we did not find group differences in the WM skeleton as defined by TBSS analysis. This suggests that considering larger or specific ROIs may be more important for detecting group differences than just the WM skeleton. However, the previously described MK-GR relationship remains unaffected by the mask used, showing consistent results for both the JHU ensemble and WM skeleton (not shown). Interestingly, the spatial localization of the strongest GR-MK significant contrasts between HC and PT (**Fig. 2D**) coincides with the FA WM ROIs (CR, genu and body of the CC) showing the strongest effect size between HC and PT found in the large meta-analysis of the ENIGMA study group[46] and similarly reported in our previous study[63].

Limitations

Our study has a few limitations that need to be considered. First, we used harmonization procedures to remove both the effects of MRI scanner and of plate readers used to quantify the redox markers. In addition, the delay between MRI acquisition and blood collection could be another source of bias[8] despite being capped and controlled during the statistical analyses. The small sample size and heterogeneity among the PT cohort (that includes early psychosis PT and subjects with chronic SZ) may significantly reduce the statistical power due to potential conflicting trends that may arise at WM microstructure or GSH-system levels across the different stages and types of psychosis. Finally, GPx and GR activities and their ratio in blood cells inform us about the systemic redox homeostasis which does not necessarily reflect the conditions found in the brain. However, it is likely that systemic redox dysregulation impact brain structure and function. Indeed, several studies have found associations of peripheral markers of the GSH-redox

cycle with brain GSH levels[95], brain atrophy and enlargement of the lateral ventricles[96], or EEG sensory evoked responses[97].

Conclusions

Altogether, our extensive association analyses indicate that while the peripheral GSH-redox cycle may predict WM microstructural properties such as MK in HC and age-dependent increase of MD in WM, it does not alone explain the WM anomalies detected in PT. Our results do not however exclude the involvement of the GSH redox cycle during the development/maturation of WM. The dysregulation of this system during brain development could still contribute to WM anomalies in psychosis.

Acknowledgments

This work was supported by the Swiss National Science Foundation (PCEFP2_194260, to I.J.; 320030_197787 to PH and YA), the National Center of Competence in Research (NCCR) "SYNAPSY - The Synaptic Bases of Mental Diseases" from the Swiss National Science Foundation (n° 51NF40 – 185897 to KQD & PC) and the Foundation Alamaya. Dr. Alameda is supported by Carigest fellowship and by Frutiger Adrian et Simone fellowship. Dr. Dwir and P. Klauser are supported by Frutiger Adrian & Simone fellowship. The authors have nothing to disclose and there are no conflicts of interest. We are grateful to Gloria Reuteler, Adeline Cottier and Morgane Baumgartner for expert technical assistance. Dr Luis Alameda thanks the Foundation Adrian and Simone Frutiger and Carigest SA Foundation for their support

References

1. Wittchen HU, Jacobi F, Rehm J, Gustavsson A, Svensson M, Jönsson B, et al. The size and burden of mental disorders and other disorders of the brain in Europe 2010. *Eur Neuropsychopharmacol J Eur Coll Neuropsychopharmacol*. 2011;21(9):655-679. doi:10.1016/j.euroneuro.2011.07.018

2. McCutcheon RA, Reis Marques T, Howes OD. Schizophrenia—An Overview. *JAMA Psychiatry*. 2020;77(2):201-210. doi:10.1001/jamapsychiatry.2019.3360

3. Dietz AG, Goldman SA, Nedergaard M. Glial cells in schizophrenia: a unified hypothesis. *Lancet Psychiatry*. 2020;7(3):272-281. doi:10.1016/S2215-0366(19)30302-5

4. Nakazawa K, Sapkota K. The origin of NMDA receptor hypofunction in schizophrenia. *Pharmacol Ther*. 2020;205:107426. doi:10.1016/j.pharmthera.2019.107426

5. Ni P, Chung S. Mitochondrial Dysfunction in Schizophrenia. *BioEssays News Rev Mol Cell Dev Biol*. 2020;42(6):e1900202. doi:10.1002/bies.201900202

6. Murphy CE, Walker AK, Weickert CS. Neuroinflammation in schizophrenia: the role of nuclear factor kappa B. *Transl Psychiatry*. 2021;11(1):528. doi:10.1038/s41398-021-01607-0

7. Howes OD, Onwordi EC. The synaptic hypothesis of schizophrenia version III: a master mechanism. *Mol Psychiatry*. 2023;28(5):1843-1856. doi:10.1038/s41380-023-02043-w

8. Perkins DO, Jeffries CD, Do KQ. Potential Roles of Redox Dysregulation in the Development of Schizophrenia. *Biol Psychiatry*. 2020;88(4):326-336. doi:10.1016/j.biopsych.2020.03.016

9. Tsugawa S, Noda Y, Tarumi R, Mimura Y, Yoshida K, Iwata Y, et al. Glutathione levels and activities of glutathione metabolism enzymes in patients with schizophrenia: A systematic review and meta-analysis. *J Psychopharmacol (Oxf)*. 2019;33(10):1199-1214. doi:10.1177/0269881119845820

10. Rambaud V, Marzo A, Chaumette B. Oxidative Stress and Emergence of Psychosis. *Antioxid Basel Switz*. 2022;11(10):1870. doi:10.3390/antiox11101870

11. Jorgensen A, Baago IB, Rygner Z, Jorgensen MB, Andersen PK, Kessing LV, et al. Association of Oxidative Stress-Induced Nucleic Acid Damage With Psychiatric Disorders in Adults: A Systematic Review and Meta-analysis. *JAMA Psychiatry*. 2022;79(9):920-931. doi:10.1001/jamapsychiatry.2022.2066

12. Kim SY, Cohen BM, Chen X, Lukas SE, Shinn AK, Yuksel AC, et al. Redox Dysregulation in Schizophrenia Revealed by in vivo NAD+/NADH Measurement. *Schizophr Bull*. 2017;43(1):197-204. doi:10.1093/schbul/sbw129

13. Das TK, Javadzadeh A, Dey A, Sabesan P, Théberge J, Radua J, et al. Antioxidant defense in schizophrenia and bipolar disorder: A meta-analysis of MRS studies of anterior cingulate glutathione. *Prog Neuropsychopharmacol Biol Psychiatry*. 2019;91:94-102. doi:10.1016/j.pnpbp.2018.08.006

14. Ma J, Li DM, Zhang R, Yang XD, Gao CG, Lu SM, et al. Genetic analysis of glutamate cysteine ligase modifier (GCLM) gene and schizophrenia in Han Chinese. *Schizophr Res*. 2010;119(1-3):273-274. doi:10.1016/j.schres.2009.12.017

15. Tosic M, Ott J, Barral S, Bovet P, Deppen P, Gheorghita F, et al. Schizophrenia and Oxidative Stress: Glutamate Cysteine Ligase Modifier as a Susceptibility Gene. *Am J Hum Genet*. 2006;79(3):586-592. doi:10.1086/507566

16. Rodríguez-Santiago B, Brunet A, Sobrino B, Serra-Juhé C, Flores R, Armengol L, et al. Association of common copy number variants at the glutathione S-transferase genes and rare novel genomic changes with schizophrenia. *Mol Psychiatry*. 2010;15(10):1023-1033. doi:10.1038/mp.2009.53

17. Gravina P, Spoletini I, Masini S, Valentini A, Vanni D, Paladini E, et al. Genetic polymorphisms of glutathione *S*-transferases GSTM1, GSTT1, GSTP1 and GSTA1 as risk factors for schizophrenia. *Psychiatry Res*. 2011;187(3):454-456. doi:10.1016/j.psychres.2010.10.008

18. Yan C, Duan L, Fu C, Tian C, Zhang B, Shao X, et al. Association Between Glutathione S-Transferase (GST) Polymorphisms and Schizophrenia in a Chinese Han Population. *Neuropsychiatr Dis Treat*. 2020;16(null):479-487. doi:10.2147/NDT.S235043

19. Gysin R, Kraftsik R, Sandell J, Bovet P, Chappuis C, Conus P, et al. Impaired glutathione synthesis in schizophrenia: Convergent genetic and functional evidence. *Proc Natl Acad Sci*. 2007;104(42):16621-16626. doi:10.1073/pnas.0706778104

20. Yao JK, Leonard S, Reddy R. Altered Glutathione Redox State in Schizophrenia. *Dis Markers*. NaN/NaN/NaN;22(1-2):83-93. doi:10.1155/2006/248387

21. Gawryluk JW, Wang JF, Andreazza AC, Shao L, Young LT. Decreased levels of glutathione, the major brain antioxidant, in post-mortem prefrontal cortex from patients with psychiatric disorders. *Int J Neuropsychopharmacol*. 2011;14(1):123-130. doi:10.1017/S1461145710000805

22. Zhang Y, Catts VS, Shannon Weickert C. Lower antioxidant capacity in the prefrontal cortex of individuals with schizophrenia. *Aust N Z J Psychiatry*. 2018;52(7):690-698. doi:10.1177/0004867417728805

23. Flatow J, Buckley P, Miller BJ. Meta-Analysis of Oxidative Stress in Schizophrenia. *Biol Psychiatry*. 2013;74(6):400-409. doi:10.1016/j.biopsych.2013.03.018

24. Fournier M, Scolamiero M, Gholam-Rezaee MM, Cleusix M, Jenni R, Ferrari C, et al. Topology predicts long-term functional outcome in early psychosis. *Mol Psychiatry*. 2021;26(9):5335-5346. doi:10.1038/s41380-020-0826-1

25. Monin A, Fournier M, Baumann PS, Cuénod M, Do KQ. Role of Redox Dysregulation in White Matter Anomalies Associated with Schizophrenia. In: *Handbook of Behavioral Neuroscience*. Vol 23. Elsevier; 2016:481-500. doi:10.1016/B978-0-12-800981-9.00028-6

26. Monin A, Baumann PS, Griffa A, Xin L, Mekle R, Fournier M, et al. Glutathione deficit impairs myelin maturation: relevance for white matter integrity in schizophrenia patients. *Mol Psychiatry*. 2015;20(7):827-838. doi:10.1038/mp.2014.88

27. Juurlink BH, Thorburne SK, Hertz L. Peroxide-scavenging deficit underlies oligodendrocyte susceptibility to oxidative stress. *Glia*. 1998;22(4):371-378. doi:10.1002/(sici)1098-1136(199804)22:4<371::aid-glia6>3.0.co;2-6

28. Bradl M, Lassmann H. Oligodendrocytes: biology and pathology. *Acta Neuropathol (Berl)*. 2010;119(1):37-53. doi:10.1007/s00401-009-0601-5

29. Thorburne SK, Juurlink BH. Low glutathione and high iron govern the susceptibility of oligodendroglial precursors to oxidative stress. *J Neurochem*. 1996;67(3):1014-1022. doi:10.1046/j.1471-4159.1996.67031014.x

30. Back SA, Gan X, Li Y, Rosenberg PA, Volpe JJ. Maturation-Dependent Vulnerability of Oligodendrocytes to Oxidative Stress-Induced Death Caused by Glutathione Depletion. *J Neurosci*. 1998;18(16):6241-6253. doi:10.1523/JNEUROSCI.18-16-06241.1998

31. Ravera S, Bartolucci M, Cuccarolo P, Litamè E, Illarcio M, Calzia D, et al. Oxidative stress in myelin sheath: The other face of the extramitochondrial oxidative phosphorylation ability. *Free Radic Res*. 2015;49(9):1156-1164. doi:10.3109/10715762.2015.1050962

446 32. Baud O, Greene AE, Li J, Wang H, Volpe JJ, Rosenberg PA. Glutathione peroxidase-catalase cooperativity is
447 required for resistance to hydrogen peroxide by mature rat oligodendrocytes. *J Neurosci Off J Soc Neurosci*.
448 2004;24(7):1531-1540. doi:10.1523/JNEUROSCI.3989-03.2004

449 33. Nave KA, Asadollahi E, Sasmita A. Expanding the function of oligodendrocytes to brain energy metabolism.
450 *Curr Opin Neurobiol*. 2023;83:102782. doi:10.1016/j.conb.2023.102782

451 34. Smith GA, Lin TH, Sheehan AE, Van der Goes van Naters W, Neukomm LJ, Graves HK, et al. Glutathione S-
452 Transferase Regulates Mitochondrial Populations in Axons through Increased Glutathione Oxidation. *Neuron*.
453 2019;103(1):52-65.e6. doi:10.1016/j.neuron.2019.04.017

454 35. Dwir D, Giangreco B, Xin L, Tenenbaum L, Cabungcal JH, Steullet P, et al. MMP9/RAGE pathway overactivation
455 mediates redox dysregulation and neuroinflammation, leading to inhibitory/excitatory imbalance: a reverse
456 translation study in schizophrenia patients. *Mol Psychiatry*. 2020;25(11):2889-2904. doi:10.1038/s41380-019-
457 0393-5

458 36. Lloyd AF, Davies CL, Miron VE. Microglia: origins, homeostasis, and roles in myelin repair. *Curr Opin*
459 *Neurobiol*. 2017;47:113-120. doi:10.1016/j.conb.2017.10.001

460 37. Uranova NA, Vikhreva OV, Rachmanova VI, Orlovskaya DD. Ultrastructural Alterations of Myelinated Fibers
461 and Oligodendrocytes in the Prefrontal Cortex in Schizophrenia: A Postmortem Morphometric Study. *Schizophr Res*
462 *Treat*. 2011;2011:e325789. doi:10.1155/2011/325789

463 38. Uranova NA, Vikhreva OV, Rakhmanova VI, Orlovskaya DD. Ultrastructural pathology of oligodendrocytes
464 adjacent to microglia in prefrontal white matter in schizophrenia. *Npj Schizophr*. 2018;4(1):1-10.
465 doi:10.1038/s41537-018-0068-2

466 39. Williams M, ed. *The Neuropathology of Schizophrenia*. Cham: Springer International Publishing; 2021.
467 doi:10.1007/978-3-030-68308-5

468 40. Uranova NA, Vikhreva OV, Rakhmanova VI, Orlovskaya DD. Dystrophy of Oligodendrocytes and Adjacent
469 Microglia in Prefrontal Gray Matter in Schizophrenia. *Front Psychiatry*. 2020;11.
470 https://www.frontiersin.org/articles/10.3389/fpsyt.2020.00204. Accessed March 10, 2023.

471 41. Beaulieu C. The basis of anisotropic water diffusion in the nervous system - a technical review. *NMR Biomed*.
472 2002;15(7-8):435-455. doi:10.1002/nbm.782

473 42. Cetin-Karayumak S, Di Biase MA, Chunga N, Reid B, Somes N, Lyall AE, et al. White matter abnormalities
474 across the lifespan of schizophrenia: a harmonized multi-site diffusion MRI study. *Mol Psychiatry*. 2020;25(12):3208-
475 3219. doi:10.1038/s41380-019-0509-y

476 43. Friedman Joseph I, Tang C, Carpenter D, Buchsbaum M, Schmeidler J, Flanagan L, et al. Diffusion Tensor
477 Imaging Findings in First-Episode and Chronic Schizophrenia Patients. *Am J Psychiatry*. 2008;165(8):1024-1032.
478 doi:10.1176/appi.ajp.2008.07101640

479 44. Barth C, Kelly S, Nerland S, Jahanshad N, Alloza C, Ambrogi S, et al. In vivo white matter microstructure in
480 adolescents with early-onset psychosis: a multi-site mega-analysis. *Mol Psychiatry*. 2023;28(3):1159-1169.
481 doi:10.1038/s41380-022-01901-3

482 45. Karlsgodt KH. White Matter Microstructure across the Psychosis Spectrum. *Trends Neurosci*.
483 2020;43(6):406-416. doi:10.1016/j.tins.2020.03.014

484 46. Kelly S, Jahanshad N, Zalesky A, Kochunov P, Agartz I, Alloza C, et al. Widespread white matter microstructural
485 differences in schizophrenia across 4322 individuals: results from the ENIGMA Schizophrenia DTI Working Group.
486 *Mol Psychiatry*. 2018;23(5):1261-1269. doi:10.1038/mp.2017.170

487 47. van Velzen LS, Kelly S, Isaev D, Aleman A, Aftanas LI, Bauer J, et al. White matter disturbances in major
488 depressive disorder: a coordinated analysis across 20 international cohorts in the ENIGMA MDD working group. *Mol*
489 *Psychiatry*. 2020;25(7):1511-1525. doi:10.1038/s41380-019-0477-2

490 48. Klauser P, Xin L, Fournier M, Griffa A, Cleusix M, Jenni R, et al. N-acetylcysteine add-on treatment leads to an
491 improvement of fornix white matter integrity in early psychosis: a double-blind randomized placebo-controlled trial.
492 *Transl Psychiatry*. 2018;8(1):1-8. doi:10.1038/s41398-018-0266-8

493 49. Conus P, Seidman LJ, Fournier M, Xin L, Cleusix M, Baumann PS, et al. N-acetylcysteine in a Double-Blind
494 Randomized Placebo-Controlled Trial: Toward Biomarker-Guided Treatment in Early Psychosis. *Schizophr Bull*.
495 2018;44(2):317-327. doi:10.1093/schbul/sbx093

496 50. Jensen JH, Helpern JA, Ramani A, Lu H, Kaczynski K. Diffusional kurtosis imaging: The quantification of non-
497 gaussian water diffusion by means of magnetic resonance imaging. *Magn Reson Med*. 2005;53(6):1432-1440.
498 doi:10.1002/mrm.20508

499 51. Jensen JH, Helpern JA. MRI quantification of non-Gaussian water diffusion by kurtosis analysis. *NMR Biomed*.
500 2010;23(7):698-710. doi:10.1002/nbm.1518

501 52. Jespersen SN, Olesen JL, Hansen B, Shemesh N. Diffusion time dependence of microstructural parameters in
502 fixed spinal cord. *NeuroImage*. 2018;182:329-342. doi:10.1016/j.neuroimage.2017.08.039

503 53. Fieremans E, Jensen JH, Helpern JA. White matter characterization with diffusional kurtosis imaging.
504 *NeuroImage*. 2011;58(1):177-188. doi:10.1016/j.neuroimage.2011.06.006

505 54. Zhang H, Schneider T, Wheeler-Kingshott CA, Alexander DC. NODDI: practical in vivo neurite orientation
506 dispersion and density imaging of the human brain. *NeuroImage*. 2012;61(4):1000-1016.
507 doi:10.1016/j.neuroimage.2012.03.072

508 55. Novikov DS, Kiselev VG, Jespersen SN. On modeling. *Magn Reson Med*. 2018;79(6):3172-3193.
509 doi:10.1002/mrm.27101

510 56. Pasternak O, Sochen N, Gur Y, Intrator N, Assaf Y. Free water elimination and mapping from diffusion MRI.
511 *Magn Reson Med*. 2009;62(3):717-730. doi:10.1002/mrm.22055

512 57. Guglielmetti C, Veraart J, Roelant E, Mai Z, Daans J, Van Audekerke J, et al. Diffusion kurtosis imaging probes
513 cortical alterations and white matter pathology following cuprizone induced demyelination and spontaneous
514 remyelination. *NeuroImage*. 2016;125:363-377. doi:10.1016/j.neuroimage.2015.10.052

515 58. Jelescu IO, Zurek M, Winters KV, Veraart J, Rajaratnam A, Kim NS, et al. In vivo quantification of demyelination
516 and recovery using compartment-specific diffusion MRI metrics validated by electron microscopy. *NeuroImage*.
517 2016;132:104-114. doi:10.1016/j.neuroimage.2016.02.004

518 59. Wang Y, Wang Q, Haldar JP, Yeh FC, Xie M, Sun P, et al. Quantification of increased cellularity during
519 inflammatory demyelination. *Brain*. 2011;134(12):3590-3601. doi:10.1093/brain/awr307

520 60. Falangola MF, Guilfoyle DN, Tabesh A, Hui ES, Nie X, Jensen JH, et al. Histological correlation of diffusional
521 kurtosis and white matter modeling metrics in cuprizone-induced corpus callosum demyelination. *NMR Biomed*.
522 2014;27(8):948-957. doi:10.1002/nbm.3140

523 61. Jelescu IO, Fieremans E. Chapter 2 - Sensitivity and specificity of diffusion MRI to neuroinflammatory
524 processes. In: Laule C, Port JD, eds. *Advances in Magnetic Resonance Technology and Applications*. Vol 9. Imaging
525 Neuroinflammation. Academic Press; 2023:31-50. doi:10.1016/B978-0-323-91771-1.00010-1

526 62. Wijtenburg SA, Rowland LM. Chapter 19 - Schizophrenia spectrum disorders. In: Laule C, Port JD, eds.
527 *Advances in Magnetic Resonance Technology and Applications*. Vol 9. Imaging Neuroinflammation. Academic Press;
528 2023:469-487. doi:10.1016/B978-0-323-91771-1.00008-3

529 63. Pavan T, Alemán-Gómez Y, Jenni R, Steullet P, Schilliger Z, Dwir D, et al. White Matter Microstructure
530 Alterations in Early Psychosis and Schizophrenia. April 2024:2024.02.01.24301979.
531 doi:10.1101/2024.02.01.24301979

532 64. Yung AR, Yuen HP, McGorry PD, Phillips LJ, Kelly D, Dell'Olio M, et al. Mapping the onset of psychosis: the
533 Comprehensive Assessment of At-Risk Mental States. *Aust N Z J Psychiatry*. 2005;39(11-12):964-971.
534 doi:10.1080/j.1440-1614.2005.01714.x

65. Kay SR, Fiszbein A, Opler LA. The Positive and Negative Syndrome Scale (PANSS) for Schizophrenia. *Schizophr Bull*. 1987;13(2):261-276. doi:10.1093/schbul/13.2.261

66. American Psychiatric Association. *Diagnostic and Statistical Manual of Mental Disorders (4th Ed., Text Rev.).*; 2000.

67. Tustison NJ, Avants BB, Cook PA, Zheng Y, Egan A, Yushkevich PA, et al. N4ITK: improved N3 bias correction. *IEEE Trans Med Imaging*. 2010;29(6):1310-1320. doi:10.1109/TMI.2010.2046908

68. Grabner G, Janke AL, Budge MM, Smith D, Pruessner J, Collins DL. Symmetric Atlasing and Model Based Segmentation: An Application to the Hippocampus in Older Adults. In: Larsen R, Nielsen M, Sporring J, eds. *Medical Image Computing and Computer-Assisted Intervention – MICCAI 2006*. Lecture Notes in Computer Science. Berlin, Heidelberg: Springer; 2006:58-66. doi:10.1007/11866763_8

69. Avants BB, Epstein CL, Grossman M, Gee JC. Symmetric diffeomorphic image registration with cross-correlation: evaluating automated labeling of elderly and neurodegenerative brain. *Med Image Anal*. 2008;12(1):26-41. doi:10.1016/j.media.2007.06.004

70. Ades-Aron B, Veraart J, Kochunov P, McGuire S, Sherman P, Kellner E, et al. Evaluation of the accuracy and precision of the diffusion parameter EStImation with Gibbs and NoisE removal pipeline. *NeuroImage*. 2018;183:532-543. doi:10.1016/j.neuroimage.2018.07.066

71. Veraart J, Sijbers J, Sunaert S, Leemans A, Jeurissen B. Weighted linear least squares estimation of diffusion MRI parameters: Strengths, limitations, and pitfalls. *NeuroImage*. 2013;81:335-346. doi:10.1016/j.neuroimage.2013.05.028

72. Johnson WE, Li C, Rabinovic A. Adjusting batch effects in microarray expression data using empirical Bayes methods. *Biostat Oxf Engl*. 2007;8(1):118-127. doi:10.1093/biostatistics/kxj037

73. R Core Team. *R: A Language and Environment for Statistical Computing*. Vienna, Austria: R Foundation for Statistical Computing; 2023. https://www.R-project.org/.

74. Maechler M, Rousseeuw P, Croux C, Todorov V, Ruckstuhl A, Salibian-Barrera M, et al. *Robustbase: Basic Robust Statistics*.; 2023. http://robustbase.r-forge.r-project.org/.

75. Martínez De Toda I, Vida C, Garrido A, De La Fuente M. Redox Parameters as Markers of the Rate of Aging and Predictors of Life Span. *J Gerontol Ser A*. February 2019. doi:10.1093/gerona/glz033

76. Jones DP, Mody VC, Carlson JL, Lynn MJ, Sternberg P. Redox analysis of human plasma allows separation of pro-oxidant events of aging from decline in antioxidant defenses. *Free Radic Biol Med*. 2002;33(9):1290-1300. doi:10.1016/S0891-5849(02)01040-7

565 77. Fortin JP, Parker D, Tunç B, Watanabe T, Elliott MA, Ruparel K, et al. Harmonization of multi-site diffusion
566 tensor imaging data. *NeuroImage*. 2017;161:149-170. doi:10.1016/j.neuroimage.2017.08.047

567 78. Alemán-Gómez Y, Najdenovska E, Roine T, Fartaria MJ, Canales-Rodríguez EJ, Rovó Z, et al. Partial-volume
568 modeling reveals reduced gray matter in specific thalamic nuclei early in the time course of psychosis and chronic
569 schizophrenia. *Hum Brain Mapp*. 2020;41(14):4041-4061. doi:10.1002/hbm.25108

570 79. Smith SM, Jenkinson M, Johansen-Berg H, Rueckert D, Nichols TE, Mackay CE, et al. Tract-based spatial
571 statistics: voxelwise analysis of multi-subject diffusion data. *NeuroImage*. 2006;31(4):1487-1505.
572 doi:10.1016/j.neuroimage.2006.02.024

573 80. Winkler AM, Ridgway GR, Webster MA, Smith SM, Nichols TE. Permutation inference for the general linear
574 model. *NeuroImage*. 2014;92:381-397. doi:10.1016/j.neuroimage.2014.01.060

575 81. Koga M, Serritella AV, Sawa A, Sedlak TW. Implications for reactive oxygen species in schizophrenia
576 pathogenesis. *Schizophr Res*. 2016;176(1):52-71. doi:10.1016/j.schres.2015.06.022

577 82. Martínez de Toda I, Vida C, Sanz San Miguel L, De la Fuente M. Function, Oxidative, and Inflammatory Stress
578 Parameters in Immune Cells as Predictive Markers of Lifespan throughout Aging. *Oxid Med Cell Longev*.
579 2019;2019:4574276. doi:10.1155/2019/4574276

580 83. Stadtman ER. Importance of individuality in oxidative stress and aging. *Free Radic Biol Med*. 2002;33(5):597-
581 604. doi:10.1016/s0891-5849(02)00904-8

582 84. Schilliger Z, Alemán-Gómez Y, Magnus Smith M, Celen Z, Meuleman B, Binz PA, et al. Sex-specific interactions
583 between stress axis and redox balance are associated with internalizing symptoms and brain white matter
584 microstructure in adolescents. *Transl Psychiatry*. 2024;14(1):1-11. doi:10.1038/s41398-023-02728-4

585 85. Raffa M, Mechri A, Othman LB, Fendri C, Gaha L, Kerkeni A. Decreased glutathione levels and antioxidant
586 enzyme activities in untreated and treated schizophrenic patients. *Prog Neuropsychopharmacol Biol Psychiatry*.
587 2009;33(7):1178-1183. doi:10.1016/j.pnpbp.2009.06.018

588 86. Abdalla DS, Monteiro HP, Oliveira JA, Bechara EJ. Activities of superoxide dismutase and glutathione
589 peroxidase in schizophrenic and manic-depressive patients. *Clin Chem*. 1986;32(5):805-807.
590 doi:10.1093/clinchem/32.5.805

591 87. Martínez de Toda I, González-Sánchez M, Díaz-Del Cerro E, Valera G, Carracedo J, Guerra-Pérez N. Sex
592 differences in markers of oxidation and inflammation. Implications for ageing. *Mech Ageing Dev*. 2023;211:111797.
593 doi:10.1016/j.mad.2023.111797

88. Dukhande VV, Isaac AO, Chatterji T, Lai JCK. Reduced glutathione regenerating enzymes undergo developmental decline and sexual dimorphism in the rat cerebral cortex. *Brain Res*. 2009;1286:19-24. doi:10.1016/j.brainres.2009.05.029

89. Ruszkiewicz JA, Miranda-Vizuete A, Tinkov AA, Skalnaya MG, Skalny AV, Tsatsakis A, et al. Sex-Specific Differences in Redox Homeostasis in Brain Norm and Disease. *J Mol Neurosci*. 2019;67(2):312-342. doi:10.1007/s12031-018-1241-9

90. Alameda L, Fournier M, Khadimallah I, Griffa A, Cleusix M, Jenni R, et al. Redox dysregulation as a link between childhood trauma and psychopathological and neurocognitive profile in patients with early psychosis. *Proc Natl Acad Sci U S A*. 2018;115(49):12495-12500. doi:10.1073/pnas.1812821115

91. Korge P, Calmettes G, Weiss JN. Increased reactive oxygen species production during reductive stress: The roles of mitochondrial glutathione and thioredoxin reductases. *Biochim Biophys Acta BBA - Bioenerg*. 2015;1847(6):514-525. doi:10.1016/j.bbabio.2015.02.012

92. Bouhrara M, Avram AV, Kiely M, Trivedi A, Benjamini D. Adult lifespan maturation and degeneration patterns in gray and white matter: A mean apparent propagator (MAP) MRI study. *Neurobiol Aging*. 2023;124:104-116. doi:10.1016/j.neurobiolaging.2022.12.016

93. Teissier T, Boulanger E, Deramecourt V. Normal ageing of the brain: Histological and biological aspects. *Rev Neurol (Paris)*. 2020;176(9):649-660. doi:10.1016/j.neurol.2020.03.017

94. Okusaga OO. Accelerated Aging in Schizophrenia Patients: The Potential Role of Oxidative Stress. *Aging Dis*. 2013;5(4):256-262. doi:10.14336/AD.2014.0500256

95. Xin L, Mekle R, Fournier M, Baumann PS, Ferrari C, Alameda L, et al. Genetic Polymorphism Associated Prefrontal Glutathione and Its Coupling With Brain Glutamate and Peripheral Redox Status in Early Psychosis. *Schizophr Bull*. 2016;42(5):1185-1196. doi:10.1093/schbul/sbw038

96. Buckman TD, Kling AS, Eiduson S, Sutphin MS, Steinberg A. Glutathione peroxidase and CT scan abnormalities in schizophrenia. *Biol Psychiatry*. 1987;22(11):1349-1356. doi:10.1016/0006-3223(87)90069-2

97. Geiser E, Retsa C, Knebel JF, Ferrari C, Jenni R, Fournier M, et al. The coupling of low-level auditory dysfunction and oxidative stress in psychosis patients. *Schizophr Res*. 2017;190:52-59. doi:10.1016/j.schres.2017.02.002

Figures and Tables

		HC (N=86)		PT (N=99)			
		Mean	Std.	Men	Std.	Stat.	p-value
Age (years)		28.1	8.6	29.0	9.4	W=3989	p=4.6e-01ns
GPx		16.7	6.6	16.2	6.1		
GR		2.5	0.7	2.3	0.7		
GPx/GR-ratio		6.9	2.7	7.3	3.2		
Delay MRI-Biomarker (days)†		17.9	31.7	39.2†	44.0†	W=2444	p=8.9e-07****
Age at Psychosis Onset (years)				23.3	7.3		
Duration of illness (months)				61.9	85.2		
CPZ-equivalent dose (mg/day)				342.1	276.8		
PANSS: total				62.4	15.2		
PANSS: positive symptoms				13.2	4.3		
PANSS: negative symptoms				16.8	5.8		
PANSS: general psychopathology				32.6	8.2		
GAF		84.9	4.1	55.7	11.6	W=7962	p=1.8e-30****
		N	Pct.	N	Pct.		
Scanner	Prisma	68	79.1	74	74.7	χ^2:0.482	p=0.488
	Trio	18	20.9	25	25.5		
Sex	Female	32	37.2	24	24.2	χ^2:3.66	p=0.056
	Male	54	62.8	75	75.8		
Reader	Infinite	66	76.7	87	87.9	χ^2:3.98	p=0.046*
	SPARK	20	23.3	12	12.1		
GPx/GR-Ratio	High	44	51.2	48	48.5		
	Low	42	48.8	51	51.5		

Table 1 Cohort demographics. P-values refer to Wilcox's tests between patients and healthy control. χ2 test is computed for the scanner, sex, and reader contingency tables. GPx and GR activities are expressed in nmoles NADPH used/min/g hemoglobin. HC: healthy controls, PT: patients, GPx: glutathione peroxidase, GR: glutathione reductase, GAF: Global Assessment of Functioning, PANSS: Positive and Negative Syndrome Scale. †: the delay MRI-biomarker statistics are reported excluding one PT participant with an extreme delay of 271 days.

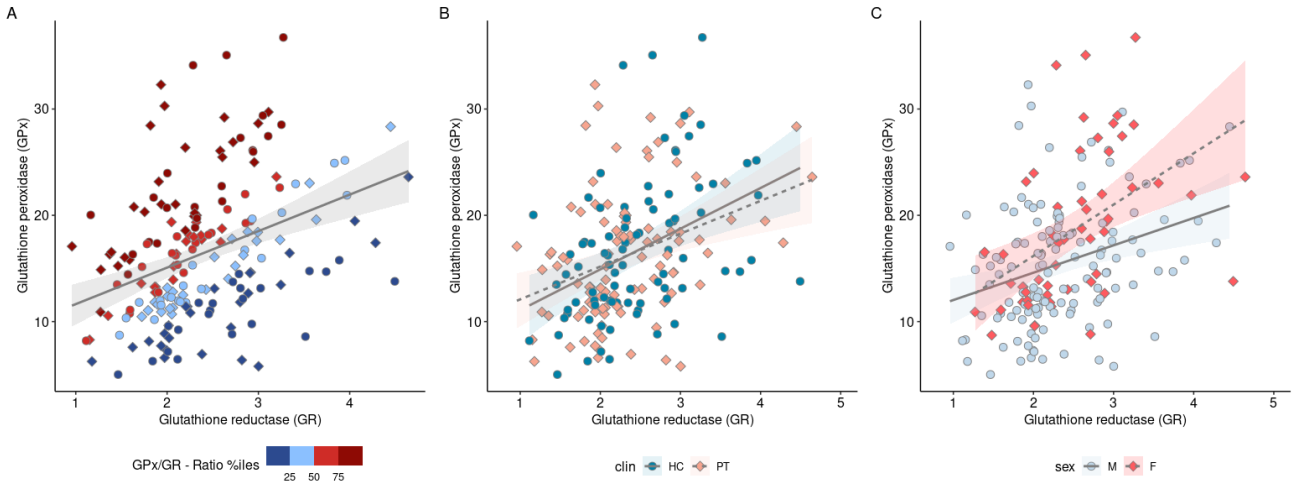

631 **Figure 1 Biomarkers of the blood GSH-redox cycle and the effects of sex and clinical status.** Correlations
632 between GPx and GR activity in the whole cohort, colored by the quartiles of the ratio between GPx and GR (A), clinical
633 status (B), and sex (C). GPx and GR activities are expressed in nmoles NADPH used/min/g hemoglobin. GPx: GSH
634 peroxidase; GR: GSH reductase; HC: healthy controls; PT: patients; M: males; F: females.

635

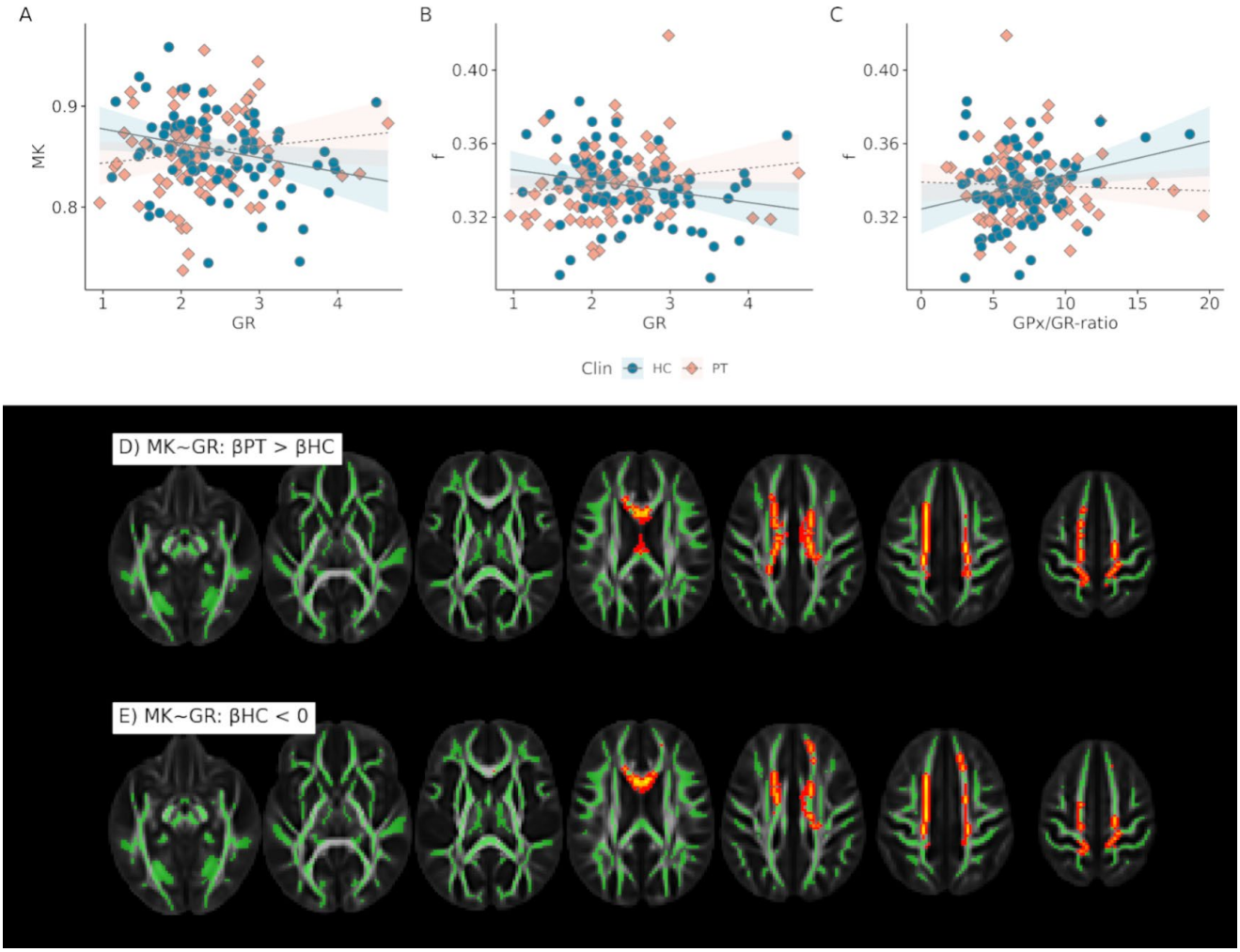

636 **Figure 2 Significant associations found between biomarkers of the blood GSH-redox cycle and the dMRI**
637 **microstructure estimates.** Scatter plots A and B show the associations between GR activity and MK (A) and *f* (B)
638 mean WM skeleton of HC (blue) vs patients (orange). Plot C shows the association of GPx/GR-ratio and *f* WM skeleton.
639 GR activity is expressed in nmoles NADPH used/min/g hemoglobin. Brain plots D and E show the results for the TBSS
640 analysis for the regressions of plot A ($p_{fdr} \leq 0.05$). GR was found significantly associated with MK in HC (E) and differed
641 from the PT slope (D). Clusters were identified in the bilateral superior corona radiata, genu and body of the corpus
642 callosum. Results are corrected for age^2, sex, and delay. GR: glutathione reductase; MK: mean kurtosis; *f*: axonal water
643 fraction; βHC: slope of HC; βPT: slope of the PT.

644

645

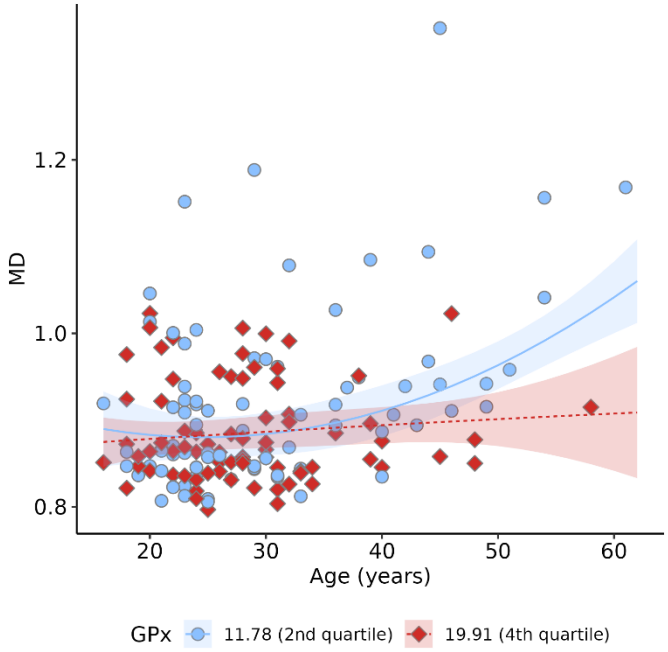

646 **Figure 3 Associations between MD and Ageing are modulated by GPx independently of the clinical status.** The
647 regression lines represent the robust fitting of the association between MD and (quadratic) age-GPx interaction, when
648 GPx is fixed at its 2nd (blue curve) and 4th quartiles (red curve). PT and HC are plotted together. At lower GPx (blue
649 curve), MD increases faster after 40 years of age than in subjects with high GPx, possibly indicating worse aging. At a
650 younger age the difference is not detectable. GPx and GR activities are expressed in nmoles NADPH used/min/g
651 hemoglobin.

652

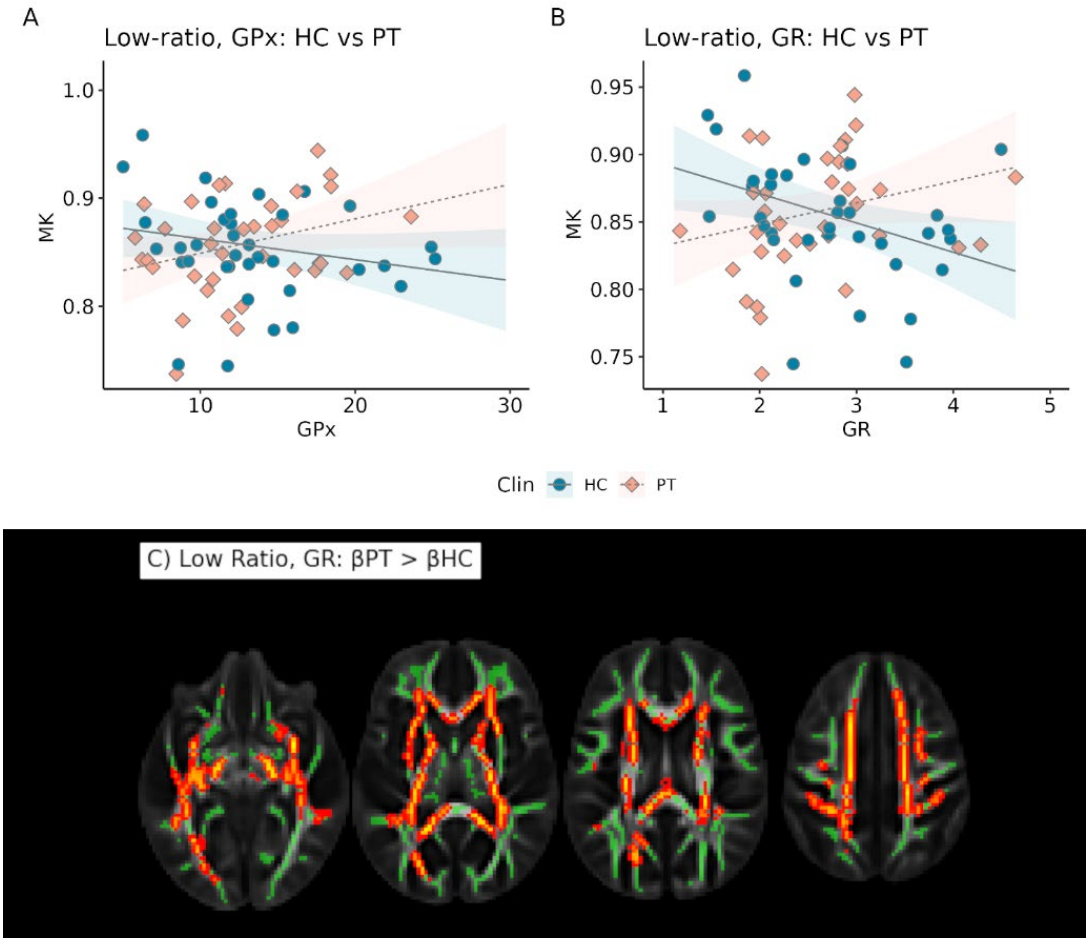

Figure 4 Associations between GR and mean kurtosis estimates among individuals with low GPx/GR-ratio. The scatterplots show the GPx (A) and GR (B) association with the MK mean-WM skeletons of individuals with low GPx/GR-ratio. GR activity is expressed in nmoles NADPH used/min/g hemoglobin. Plot (C) shows the TBSS analysis results of the same associations. In red/yellow are plotted the significant voxels ($p_{fdr} \leq 0.05$) of the contrast between the slopes of HC and PT. Both analyses included a correction for quadratic age, sex and delay. GPx and GR activities are expressed in nmoles NADPH used/min/g hemoglobin. Green: WM skeleton; HC: healthy controls; PT: patients; GR: glutathione reductase; GPx: GSH peroxidase; MK: mean kurtosis; βHC: slope of HC; βPT: slope of the PT; Low: participants with GPx/GR-ratio < median ratio of the HC group.